Tellus (1993), *45A*, 54–71

On radiating baroclinic instability of zonally varying flow

By CATHERINE A. FINLEY* and TERRENCE R. NATHAN[1], *Atmospheric Science Program, University of California, Davis, CA 95616, USA*

(Manuscript received 7 February 1992; in final form 22 June 1992)

ABSTRACT

The baroclinic instability characteristics of zonally varying flow are examined in a quasigeostrophic, two-layer, beta-plane model. The most unstable eigenmode is determined numerically by solving a one-dimensional initial value problem. Emphasis is placed on determining how the basic state vertically averaged wind, U_B, local maximum in vertical wind shear, ΔU_T, and length of the locally unstable region, λ_L, combine to yield local instabilities whose energy fluxes radiate deep into the locally neutral far field. The existence of such zonally radiating instabilities (RIs), which represent a transition between trapped and global instabilities, requires that λ_L not exceed some critical value and that $\Delta U_T/U_B$ lie within a certain range. In sharp contrast to the trapped and global instabilities, the RIs have horizontal wavelengths that increase dramatically with distance from the locally unstable region. If λ_L and $\Delta U_T/U_B$ are both sufficiently small, the local instability that emerges is characterized by a vertical asymmetry in its *horizontal* spatial structure; the disturbance in the upper layer has a longer zonal wavelength than its counterpart in the lower layer. For slowly varying basic states, analysis of the local disturbance energetics reveals that the baroclinic energy conversion predominates within the locally unstable region. For basic states that vary rapidly in the downstream direction, the barotropic energy conversion associated with the horizontal deformation field may predominate over the baroclinic conversion depending on the relative importance of ΔU_T and U_B. For RIs, the energy budget outside the locally unstable region is primarily due to the advection of total energy and the convergence of mechanical energy flux. Calculations of the basic state tendencies show that the net effect of the local (trapped or radiating) instabilities is to redistribute energy from the baroclinic to the barotropic component of the basic state flow. The fluxes produced by the trapped modes reduce the vertical shear downstream of the jet center, while the fluxes produced by the radiating modes reduce the vertical shear both downstream and near the jet center.

1. Introduction

In recent years several studies have sought to explain the observed regional development of midlatitude cyclone waves by analyzing the linear instability properties of *zonally varying* flows in idealized model atmospheres (e.g., Frederiksen, 1979; Niehaus, 1981; Pierrehumbert, 1984; Grotjahn, 1984; Peng and Williams, 1987; Cai and Mak, 1990; Crum and Stevens, 1990; Whitaker and Barcilon, 1992a, b). These stability studies have generally focused on one or a combination of two distinct classes of modes: global or local. Global modes are sensitive to the domain averaged baroclinicity and require periodic (i.e., energy recycling) boundary conditions. In contrast, local modes are insensitive to the domain averaged baroclinicity and do not require periodic boundary conditions; they are typically anchored near the jet core, extending farther downstream than upstream.

Local instabilities may be further classified as *trapped* or *radiating* depending on their ability to extend their influence beyond the locally unstable region. Trapped instabilities are confined primarily to the unstable region, exhibiting little penetration into the adjacent neutral field, whereas radiating instabilities may propagate energy well beyond the source of the instability. The existence

* Current affiliation: Department of Atmospheric Science, Colorado State University, Fort Collins, CO 80523, USA.

[1] Corresponding author.

of radiating instabilities requires that disturbances generated within a well defined unstable region have phase speeds and wavenumbers that match those of freely propagating disturbances in the neutral far field (McIntyre and Weissman, 1978). Provided such conditions are satisfied, temporally amplifying radiating waves whose amplitude envelopes slowly decay with distance from the source region may emerge.

Previous studies examining radiating instabilities in *quasi-geostrophic* baroclinic systems have focused primarily on *parallel* zonal flows in which localized supercritical regions support *meridionally* radiating disturbances (e.g., Talley, 1983). The problem of zonally varying flows supporting *zonally* radiating disturbances has yet to be fully explored and may be of particular relevance to the genesis of free waves in the atmosphere. In particular, it seems plausible that baroclinic waves generated within the major oceanic storm tracks may, under certain flow conditions, be capable of exciting free Rossby waves in the far field and radiating significant energy downstream of the source region, possibly leading to secondary development of the disturbance field. Such secondary development due to the radiation of energy has recently been noted by Orlanski and Katzfey (1991) in a study of the life cycle of a cyclone wave in the Southern Hemisphere. However, the specific background flow characteristics that favor radiating baroclinic instabilities over trapped or global baroclinic instabilities remain unclear.

The emergence of trapped, radiating or global baroclinic instabilities within zonally varying flows depends critically on the time that a disturbance resides in a locally unstable region; that time and the type of instability that occurs is greatly influenced by the length of the locally unstable region, and the relative importance of the barotropic (vertically averaged) and baroclinic (vertically sheared) parts of the basic flow. Although several of the studies cited above have considered various aspects of these flow features in examining the regional development of baroclinic disturbances, relatively little attention has been given to the factors that delineate zonally radiating baroclinic instabilities from trapped or global baroclinic instabilities. Thus we consider here a simple model of the atmosphere and examine the stability properties of an idealized zonally varying flow, placing particular emphasis on determining the differences in structural characteristics, growth rates, energetics, and basic state tendencies between zonally radiating baroclinic instabilities and trapped and global baroclinic instabilities.

2. The model

2.1. Governing equations

The baroclinic instability properties of a zonally varying flow are examined within the context of the conventional two-layer model. Briefly, the top and bottom boundaries are assumed to be flat and rigid, and the model domain lies on an infinite β-plane centered at 45° N. This model atmosphere is governed by the *linearized* quasigeostrophic potential vorticity equation, which can be written in the nondimensional form (Pedlosky, 1987)

$$\frac{\partial q_j}{\partial t} + J(\bar{\psi}_j, q_j) + J(\varphi_j, Q_j) = -R(x)\, q_j, \tag{2.1}$$

where

$$Q_j = \nabla^2 \bar{\psi}_j - (-1)^j F(\bar{\psi}_2 - \bar{\psi}_1) + \beta y, \tag{2.2a}$$

$$q_j = \nabla^2 \varphi_j - (-1)^j F(\varphi_2 - \varphi_1), \tag{2.2b}$$

represent the basic state and perturbation potential vorticities in the upper ($j=1$) and lower ($j=2$) layers, respectively. The perturbation streamfunction is $\varphi_j(x, y, t)$, and the basic state streamfunction is $\bar{\psi}_j(x, y)$, which in the absence of perturbations satisfies the steady state equation,

$$J(\bar{\psi}_j, Q_j) = \bar{G}_j, \tag{2.3}$$

where $\bar{G}_j$ represents the net forcing and dissipation. Although the nature of the forcing as well as the basic flow configuration may have an effect on the stability of the system (Andrews, 1984; Howell and Nathan, 1990), we follow Frederiksen (1983), Manney and Nathan (1990) and Whitaker and Barcilon (1992a, b), among others, and specify the basic state, $\bar{\psi}$, rather than consider the detailed nature of the forcings that produce it.

In the governing equations the key non-dimensional parameters are F, the internal rotational Froude number, and β, the planetary vorticity factor. The operators appearing in (2.1) and (2.3) are $\nabla^2 = \partial_{xx} + \partial_{yy}$ and $J(A, B) = A_x B_y - A_y B_x$.

The sole source of damping in the model is an x-dependent sponge region which varies as

$$R(x) = \hat{R} \exp\left[-\left(\frac{x-10}{1.5}\right)^2\right], \qquad (2.4)$$

where $\hat{R}$ is the amplitude of the dissipation. Physically, the sponge region absorbs any disturbance energy that wraps around the domain, thus suppressing global modes and in some instances artificially localizing local modes that extend far enough downstream to wrap around the periodic domain. Thus the sponge region serves as an artifice to distinguish between local and global modes.

The basic state and disturbance streamfunctions are chosen of the form,

$$\begin{Bmatrix} \bar{\psi} \\ \varphi \end{Bmatrix} = \begin{Bmatrix} -U_j(x)\, y \\ f_j(x, t) \cos(ly) \end{Bmatrix}, \qquad (2.5\text{a, b})$$

where the disturbance is assumed to vary slowly in the meridional direction, corresponding to $l \ll 1$. Insertion of (2.5) into (2.1) and neglecting terms of $O(l)$ yields

$$\left(\frac{\partial}{\partial t} + U_j \frac{\partial}{\partial x} + R(x)\right)\left[\frac{\partial^2 f_j}{\partial x^2} - (-1)^j F(f_2 - f_1)\right]$$
$$= \underbrace{\frac{\partial f_j}{\partial x}\left[\frac{\mathrm{d}^2 U_j}{\mathrm{d}x^2}\right.}_{\mathrm{I}} \left. + (-1)^j F(U_1 - U_2) - \beta\right]. \qquad (2.6)$$

The simplification associated with the small l approximation is immediately apparent: eq. (2.6) is independent of y and remains as such over time periods $t \lesssim O(l^{-1})$. In a WKB analysis, where the basic state is assumed to vary slowly in the zonal direction, the meridional advection of basic state relative vorticity by the disturbance field (term I) is systematically scaled out of the equation.

To facilitate interpretation of the numerical results to be presented later, we shall also consider the vertically and meridionally averaged local disturbance energetics equation, which, for $l \ll 1$, takes the form,

$$\underbrace{\frac{\partial}{\partial t}\left[\sum_{j=1}^{2} (\mathrm{KE})_j + \mathrm{PE}\right]}_{A}$$
$$= \underbrace{-\left[\sum_{j=1}^{2} U_j \frac{\partial(\mathrm{KE})_j}{\partial x} + \frac{(U_1 + U_2)}{2}\frac{\partial(\mathrm{PE})}{\partial x}\right]}_{B}$$
$$\underbrace{-\sum_{j=1}^{2}\left[v_j \frac{\partial \phi_j'}{\partial y} + \frac{\partial}{\partial x}(f_j u_j')\right]}_{C}$$
$$+ \underbrace{\sum_{j=1}^{2} \frac{\mathrm{d}U_j}{\mathrm{d}x} v_j^2}_{D} + \underbrace{2F(U_1 - U_2)(f_1 - f_2)(v_1 + v_2)}_{E}, \qquad (2.7)$$

where $\mathrm{KE}_j = v_j^2/2 = (\partial f_j/\partial x)^2/2$ is the kinetic energy and $\mathrm{PE} = (f_1 - f_2)^2 F/2$ is the available potential energy; ϕ_j' and u_j' represent the ageostrophic pressure and zonal wind fields, respectively, while v_j represents the north-south geostrophic wind. Eq. (2.7) states that the local time rate of change of total disturbance energy (term A) results from two energy redistribution processes (terms B and C) and from two energy conversion processes (terms D and E). Term B represents the advection of total disturbance energy, term C represents convergence of mechanical energy flux arising from the work done by the ageostrophic pressure and wind fields, term D represents the barotropic energy conversion associated with the horizontal deformation field, $\mathrm{d}U_j/\mathrm{d}x$, and term E represents the baroclinic energy conversion associated from the vertically sheared zonal wind, $U_1 - U_2$. A detailed derivation of (2.7) is given in the Appendix along with a description of the procedure used to calculate term C. Additional details concerning the physical interpretation of (2.7) can be found in Cai and Mak (1990).

2.2. Basic states

To simulate the zonal modulation of baroclinicity observed in the atmosphere at middle latitudes, basic state flows were chosen to consist of zonally varying baroclinic *and* barotropic components, viz.,

$$U_j(x) = [U_\mathrm{B}(x) - (-1)^j U_\mathrm{T}(x)]/2, \qquad (2.8)$$

where the baroclinic component, $U_T = U_1 - U_2$, and barotropic component, $U_B = U_1 + U_2$, were chosen of the form

$$\begin{Bmatrix} U_T(x) \\ U_B(x) \end{Bmatrix} = \begin{Bmatrix} U_{Tb} + \Delta U_T \\ U_{Bb} + \Delta U_B \end{Bmatrix} \times \left[\frac{\tanh((x-z)/z) - \tanh((x+z)/z)}{2\tanh(-1)} \right] \qquad (2.9)$$

where

$$\Delta U_T = U_{T0} - U_{Tb}, \qquad (2.10a)$$

$$\Delta U_B = U_{B0} - U_{Bb}. \qquad (2.10b)$$

Here U_{T0} is the maximum vertical shear at the jet center, $x = 0$, U_{Tb} is the value of the vertical shear outside of the jet region, U_{B0} is the value of the maximum barotropic wind at the jet center, and U_{Bb} is the barotropic wind outside the jet region. The parameter Z controls the length of the jet. Provided $\Delta U_T \neq 0$ and $\Delta U_B \neq 0$, the barotropic and baroclinic winds have the same zonal structure. For the remainder of this study the primary focus shall be on basic flows for which the barotropic wind is uniform ($\Delta U_B = 0$) and the vertical shear outside the jet region is zero ($U_{Tb} = 0$).

3. Linear stability problem

3.1. Parameters and numerical procedure

The stability of our model atmosphere was examined over a wide range of geophysically relevant parameters and basic state flow configurations. Values of $5 \leqslant F \leqslant 25$ and $1 \leqslant \beta \leqslant 5$ were chosen producing qualitatively similar results. For the remainder of this study we choose as representative values $F = 10$ and $\beta = 2.5$, corresponding to characteristic length, depth, velocity and time scales of 10^6 m, 10^4 m, 10 m/s and 10^5 s, respectively. We note that the ratio β/F corresponds to the minimum critical shear required for instability of *zonally uniform* flow in the two-layer model. While this ratio, termed the Phillips criterion after Phillips (1954), is useful in determining the onset of instability of zonally uniform flow, it cannot be used to predict the *type* of instability (local or global) that may occur in zonally varying flow.

The nondimensional domain extends from $-14 \leqslant x \leqslant 14$, corresponding to a dimensional midlatitude channel length of $\sim$28,000 km. The ranges for the jet parameters were guided by observations of the 500 mb and 850 mb flow fields from various seasons: mean wind $0 \leqslant U_B \leqslant 3$ (30 m/s), maximum vertical shear 0.25 (2.5 m/s) $\leqslant U_{T0} \leqslant 3.0$ (30 m/s), vertical shear downstream of the jet $0 \leqslant U_{Tb} \leqslant 2.0$ (20 m/s), and 0.1 (100 km) $\leqslant Z \leqslant 4.0$ (4,000 km).

The imposition of zonally periodic boundary conditions permits us to represent the streamfunction fields in spectral form using the following Fourier basis functions:

$$\begin{Bmatrix} U_j(x) \\ f_j(x,t) \end{Bmatrix} = \sum_{k=-n}^{n} \begin{Bmatrix} A_j(k) \\ a_j(k,t) \end{Bmatrix} \times \exp\left(\frac{i\,2\pi kx}{L_d}\right), \qquad j = 1, 2, \qquad (3.1)$$

where L_d is the nondimensional length of the domain; A_j and a_j are the complex spectral amplitudes of the basic state and disturbance, respectively. Here k is the non-dimensional zonal wavenumber in the computational domain, where k is related to the dimensional zonal wavenumber K by $K = (L_d/2\pi)k$. For the cases to be presented here a disturbance resolution of $n = 282$ was used, beyond which there was no detectible change in the results.

Insertion of (3.1) into (2.6) yields a system of $2n+1$ coupled equations for the disturbance amplitudes, a_j. Evaluating the advection terms using spectral transforms, the resulting system was integrated forward in time using a fourth order Runge-Kutta scheme until the *most unstable* eigenmode emerged having the form,

$$\mathrm{Re}[f_j(x,t)] = [\mathrm{Re}[a_j(x)]\cos(\omega_r t) - \mathrm{Im}[a_j(x)]\sin(\omega_r t)]\exp(\omega_i t). \qquad (3.2)$$

The frequency, ω_r, was obtained using a longitude-time plot of the eigenmode field, (3.2), whereas the growth rate, ω_i, was calculated from the disturbance kinetic energy tendency, which was averaged over all possible phases of the disturbance in order to remove periodic fluctuations arising from disturbance propagation.

For all of the integrations a time step of 0.025

was used, and the initial disturbance field was centered at $x = -7$ and chosen of the form

$$\begin{Bmatrix} f_1(x,0) \\ f_2(x,0) \end{Bmatrix} = \begin{Bmatrix} 0 \\ 0.001 \left[\dfrac{\tanh\left(\dfrac{(x+7)-0.2}{0.2}\right) - \tanh\left(\dfrac{(x+7)+0.2}{0.2}\right)}{2\tanh(-1)} \right] \end{Bmatrix}. \tag{3.3}$$

The structure of the resulting eigenmode was found to be independent of the initial position of the disturbance.

3.2. *Trapped versus radiating instabilities*

Before considering the detailed solution of (2.5)–(2.7), we briefly describe the criteria used here in distinguishing between trapped and radiating instabilities. As stated in the Introduction, the existence of radiating instabilities requires that unstable disturbances originating within a well defined source region have phase speeds and wavenumbers that match those of freely propagating Rossby waves in the locally neutral far field. Except for highly idealized basic states that yield simple dispersion relations within and outside the locally unstable region, this matching requirement is difficult to apply, particularly for the smoothly varying zonal flows examined here. Thus we consider an alternative approach and define radiating modes by the following criteria. First, we require that the spectral energetics of the disturbance field exhibit an isolated maximum,. indicative of the excitation of a free Rossby wave in the far field. Second, we require the ratio of the energy redistribution terms [B plus C in (2.7)] to the energy conversion mechanisms [D plus E in (2.7)] to exceed a critical value over a distance twice that of the locally unstable region. Stated mathematically,

$$\mathfrak{R} \equiv \frac{|B| + |C|}{|D| + |E|} > \mathfrak{R}_c \tag{3.4}$$

defines radiating modes provided $\lambda > 2\lambda_L$, where λ is the distance over which $\mathfrak{R}$ exceeds the critical value $\mathfrak{R}_c$, and λ_L is the width of the locally unstable region as determined from the local Phillip's criterion. Although disturbances may still radiate energy for $\mathfrak{R} < \mathfrak{R}_c$ or $\lambda < 2\lambda_L$, the radiated energy is confined to the locally unstable region, leaving the far field essentially unaffected. We have found the existence of the radiating instabilities to be quite robust to changes in $\mathfrak{R}_c$, which was varied from 1 to 50. For the cases to be presented $\mathfrak{R}_c = 25$.

3.3. *Results*

Displayed in figs. 1–3 are the amplitudes, ensemble averaged* energy budgets, and kinetic energy spectra of the local instabilities that arise for various combinations of barotropic wind U_B and jet length Z. Unless otherwise stated, the remaining parameters are fixed at $U_{Tb} = 0$, $U_{T0} = 1$ (10 m/s), $\Delta U_B = 0$ and $\Delta U_T = 1.0$ (10 m/s), a parameter setting for which the basic state is locally neutral outside the jet region.

Fig. 1 shows a typical trapped instability that emerges when the barotropic wind is weak [$U_B = 0.1$ (1 m/s)] and the jet is short [$Z = 0.2$ (200 km); $\lambda_L = 0.8$ (800 km)]. The disturbance in this case attained eigenmode form at $t = 57.5$ (66.5d), having growth rate $\omega_i = 0.43$ ($0.37 d^{-1}$) and frequency $\omega_r = -7.8 \times 10^{-3}$ ($6.74 \times 10^{-3} d^{-1}$). As shown in Fig. 1a, the disturbance is characterized by upper and lower layer amplitudes that are maximized near the edge of the locally unstable region; the amplitude maximum in the upper layer is about five times larger than that of the lower layer. A prominent feature, one that is characteristic of all disturbances that arise from (zonally) narrow jets and weak barotropic winds, is the vertical asymmetry in the *horizontal* spatial structure of the disturbance; the upper layer disturbance has fewer internal nodes and thus a longer zonal length* than its counterpart in the lower layer; this feature becomes more pronounced as the length of the locally unstable region decreases.

* The ensemble average is defined as a time average over all possible phases of the disturbance. For a disturbance that assumes the form of an eigenmode, the ensemble average of two disturbance quantities, say, M and N, is $[MN]_e = \mathrm{Re}(M)\,\mathrm{Re}(N) + \mathrm{Im}(M)\,\mathrm{Im}(N)$, where Re and Im denote real and imaginary parts, respectively.

* Here we define the eigenmode (zonal) length as the length of the region in which the amplitude envelope exceeds a threshold value of 0.05, where the maximum amplitude is normalized to 1.

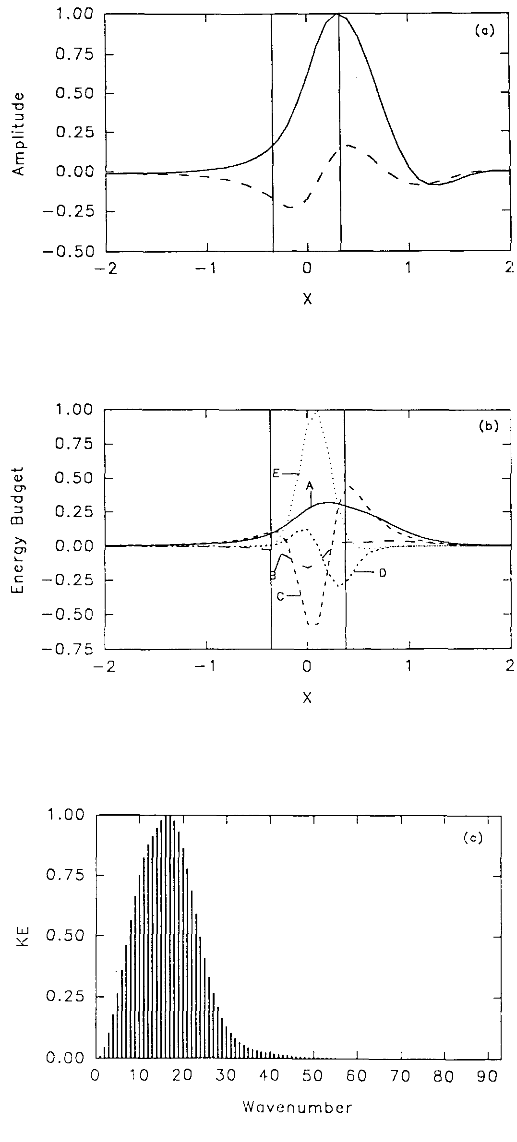

Fig. 1. Normalized structural characteristics, ensemble averaged energetics and kinetic energy spectrum of the trapped mode corresponding to $U_B = 0.1$, $Z = 0.2$ ($\lambda_L = 0.8$), and $t = 57.5$: (a) Disturbance amplitude f_j in the lower (dashed line) and upper (solid line) layers; (b) total energy tendency (solid line; A), advection of total energy (long dashed line; B), convergence of mechanical energy flux (medium dashed line; C), barotropic conversion (short dashed line; D), baroclinic conversion (dotted line; E); and (c) kinetic energy spectrum. For clarity only the range from $x = -2$ to $x = 2$ is shown in (a) and (b). The region within the vertical lines corresponds to the locally unstable region.

A similar result has been obtained by Samelson and Pedlosky (1990), but in their study the local supercriticality of *zonally uniform* flow was induced by varying the meridional slope at the lower rigid boundary.

The disturbance streamfunction amplitudes shown in Fig. 1a represent a snapshot, i.e., they correspond to that time when the disturbance has achieved the form of an eigenmode. At subsequent times there will be changes in the shape of the normalized amplitudes due to the phase propagation of the disturbance. The *location* of the amplitude envelope, however, remains fixed, which is characteristic of all the local (trapped and radiating) instabilities obtained here.

The ensemble averaged energy budget for the trapped disturbance shown in Fig. 1a is displayed in Fig. 1b. The baroclinic energy converson (E) is predominately positive and large (relative to the other processes) throughout the locally unstable region and maximized slightly downstream of the jet center where the westward displacement of the upper wave relative to the lower one is maximized. The energy redistribution processes, i.e., the advection of energy (B) and the convergence of mechanical energy flux (C) are co-located and augment (oppose) the baroclinic energy conversion for $x < (>) 0$. The barotropic energy conversion (D) is asymmetric about $x = 0$; it is relatively small and positive for $x < 0$ and about twice as large and negative for $x > 0$. By substituting (2.8) into term D in (2.7) and rearranging, the barotropic energy conversion term can be cast in a form in which its sign can be easily inferred from the structure of the disturbance, viz.,

$$D = \frac{1}{2} \frac{\mathrm{d}U_T}{\mathrm{d}x} (v_1^2 - v_2^2). \tag{3.5}$$

Thus, because $\mathrm{d}U_T/\mathrm{d}x$ is positive (negative) upstream (downstream) of the jet maximum at $x = 0$, it is clear from (3.5) that if the upper layer meridional wind is greater (smaller) than that in the lower layer, the disturbance extracts energy from the zonally sheared part of the basic state.

The corresponding kinetic energy spectrum, shown in Fig. 1c, is broad and maximized at $k \approx 16, 17$, dropping off to about half of the maximum value for $k \approx 7, 8$ and $k \approx 23$.

Consider next the radiating instability shown in Fig. 2a for $U_B = 0.5$ (5 m/s); the remaining

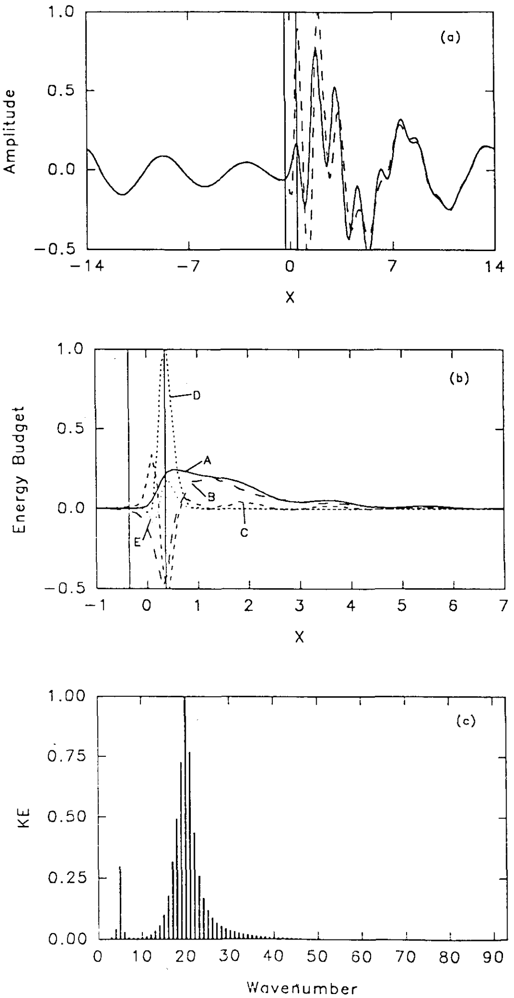

Fig. 2. As in Fig. 1 except for the radiating mode corresponding to $U_B = 0.5$, $Z = 0.2$ ($\lambda_L = 0.8$), and $t = 70$; Note the different zonal ranges between (a) and (b).

parameters are as in Fig. 1. The growth rate and frequency are $\omega_i = 0.21$ ($0.18\,\mathrm{d}^{-1}$) and $\omega_r = -5.85 \times 10^{-2}$ ($5.1 \times 10^{-2}\mathrm{d}^{-1}$), respectively. The growth rate is about half that of the trapped mode shown in Fig. 1. Although the barotropic wind, U_B, is the only different parameter from that used in Fig. 1, there are pronounced differences in structure and energetics between the trapped and radiating instabilities. For example, the radiating instability is characterized by three local amplitude maxima of comparable magnitude: the first is located at the edge of the locally unstable region, while the second and third are located, respectively, ~ 1000 km and ~ 2000 km farther downstream in the locally neutral region. As discussed in detail below, the large local wave amplitudes that extend well beyond the locally unstable region are due to the advection and radiation of energy, which become more pronounced as the width of the locally unstable region decreases. The characteristic wavelength, λ_C (measured crest to crest), and the ratio of the upper to lower layer amplitudes, f_1/f_2, changes dramatically with distance from the source region. Near the source region $\lambda_C \approx 2000$ km and $f_1/f_2 \approx 0.2$, while sufficiently far downstream the disturbance acquires a barotropic structure with $\lambda_C \approx 6000$ km and $f_1/f_2 \approx 1$.

The ensemble averaged energy budget for the radiating wave also is sharply different from that of the trapped wave (compare Figs. 1b and 2b, but note the difference in horizontal scale). For the radiating wave the barotropic energy conversion (D) is largest and positive downstream of the jet maximum and is confined to the edge of the locally unstable region; the baroclinic energy conversion (E) is negligible. In sharp contrast, the barotropic conversion for the trapped wave was negative downstream of the jet center and of secondary importance compared to the baroclinic conversion. Calculations have shown that for relatively short jets, the predominance of either the barotropic or baroclinic energy conversion processes depends crucially on the local supercriticality and the mean barotropic wind, whereas for jets that are slowly varying (in a WKB sense), the horizontal deformation field $\mathrm{d}U_j/\mathrm{d}x$ is sufficiently weak so that the baroclinic conversion always predominates. Outside the locally unstable region the sole contributions to the local energy tendency for the radiating instability are from the advection of energy (B) and the energy flux (C), which decay from their maximum value at $x \approx 1$, eventually reaching zero over a distance $\sim 6\lambda_L$.

The KE spectrum shown in Fig. 2c is maximized at $k = 20$; however, in contrast to the KE spectrum of the trapped wave shown in Fig. 1c, the spectrum for the radiating instability is more sharply peaked and, more importantly, there is an isolated maximum at $n = 5$, indicative of the excitation of the Rossby wave in the locally neutral far field. The existence of an isolated maximum in the spectral energetics is characteristic of all the radiating instabilities.

The local instabilities that arise for a slowly varying jet [$Z = 2.0$ (2000 km); $\lambda_L = 7$ (7000 km)] are shown in Fig. 3 for $U_B = 0.1$ (1 m/s; left column) and $U_B = 0.5$ (5 m/s; right column). Except for the increase in Z, the parameter settings for the $U_B = 0.1$ (1 m/s) and $U_B = 0.5$ (5 m/s) cases correspond to the trapped and radiating instabilities shown in Figs. 1, 2, respectively. Both instabilities shown in Fig. 3 are trapped and have similar spatial structures, energy budgets, and kinetic energy spectra. Within the locally unstable region the baroclinic energy conversion dominates, which is opposed primarily by the advection of energy (B) and convergence of

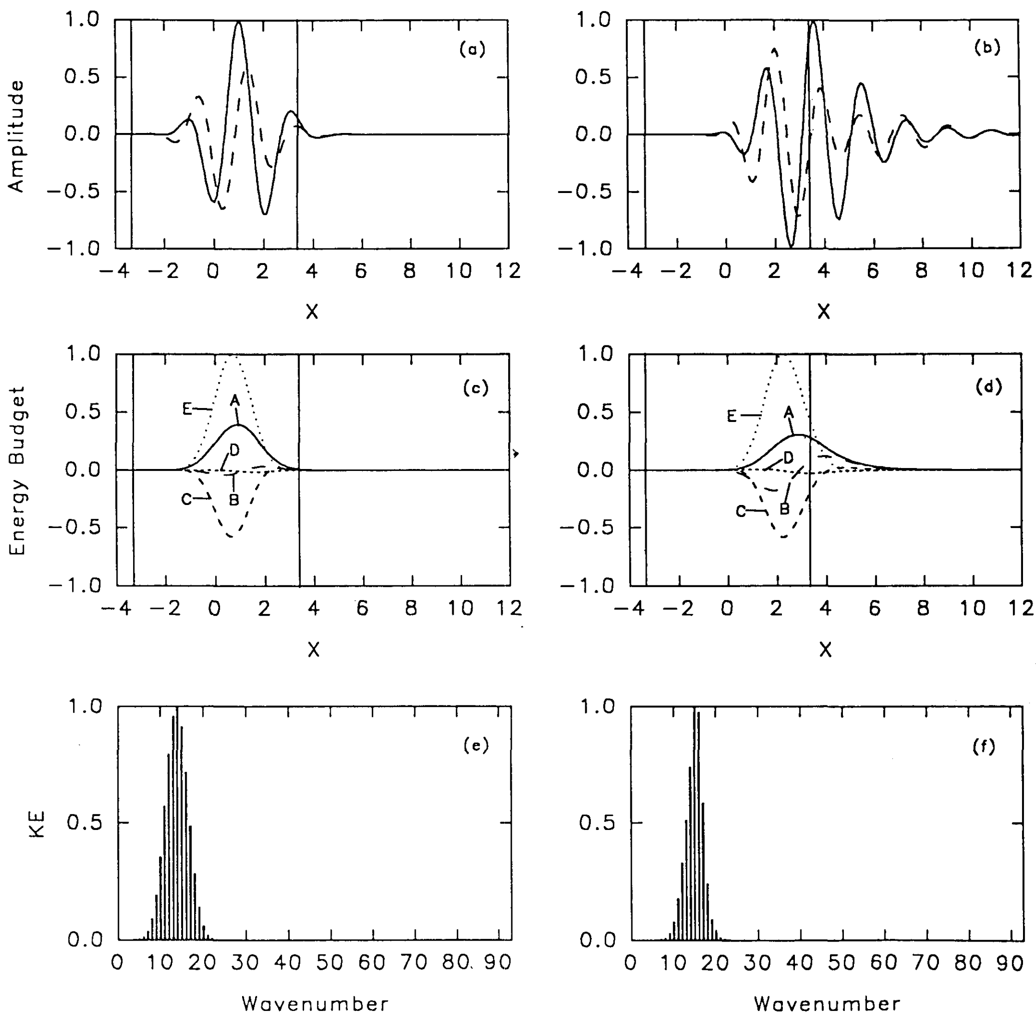

Fig. 3. Normalized structural characteristics, ensemble averaged energetics and kinetic energy spectrum of the trapped mode corresponding to $U_B = 0.1$ and $t = 29$ (left column) and $U_B = 0.5$ and $t = 34$ (right column) for $Z = 2.0$ ($\lambda_L = 7.0$). (a), (b) Disturbance amplitude f_j in the lower (dashed line) and upper (solid line) layers; (c), (d) total energy tendency (solid line; A), advection of total energy (long dashed line; B), convergence of mechanical energy flux (medium dashed line; C), barotropic conversion (short dashed line; D), baroclinic conversion (dotted line; E); and (e), (f) kinetic energy spectra. For clarity only the range from $x = -4$ to $x = 12$ is shown in (a)–(d). The region within the vertical lines corresponds to the locally unstable region.

mechanical energy flux (C). As the barotropic wind U_B increases from 0.1 to 0.5, the disturbance becomes less localized, anchors further downstream from the jet center, decreases in growth rate from $\omega_i = 0.69$ ($0.59d^{-1}$) to $\omega_i = 0.30$ ($0.26d^{-1}$) and slightly increases in frequency from $\omega_r = -3.28 \times 10^{-3}$ ($2.8 \times 10^{-3}d^{-1}$) to $\omega_r = 1.12 \times 10^{-2}$ ($9.68 \times 10^{-3}d^{-1}$).

As comparison of Figs. 1, 2 and 3 shows, the structure and energetics of the instabilities depend vitally on the barotropic wind U_B and jet length Z (or λ_L). To further examine the influence of jet length on the stability of the system, we introduce the non-dimensional parameter,

$$\alpha = \frac{\lambda_L}{\lambda_m}, \tag{3.6}$$

where λ_m is the wavelength of the most unstable plane wave corresponding to the average vertical shear in the unstable region. For $\alpha < O(1)$, the characteristic zonal length of the jet is less than that of the disturbance; this case corresponds to the WKB limit.

Displayed in Fig. 4 is the disturbance growth rate ω_i as a function of Z and α for three values of the barotropic wind: $U_B = 0.1$, 0.3, and 0.5. Also indicated on the figure are the ranges of Z and α over which the instabilities are radiating or trapped. For $Z \gtrsim O(1)$, the growth rate shows little variation with changes in jet length. This is consistent with the findings of Pierrehumbert (1984) who showed that for slowly varying zonal flows, the local mode growth rate, which is equal to the absolute growth rate determined locally at the point of maximum vertical shear, is insensitive to changes in jet length. A particularly striking feature of Fig. 4 is the large growth rates that are obtained for $\alpha < O(1)$, a parameter setting that is inaccessible to a WKB analysis. Consider, for example, the case $U_B = 0.3$. As Z decreases below about 0.3, the growth rate of the wave rapidly increases, a result that initially seems counterintuitive, since the width of the region that is locally baroclinically unstable also decreases. However, inspection of (3.5) reveals that the barotropic energy conversion, measured by the basic state deformation field dU_T/dx, is proportional to Z^{-1}, so that $dU_T/dx \to \infty$ as $Z \to 0$. Thus, unless compensated for by structural changes in the disturbance, particularly $(v_1^2 - v_2^2)$, which is sensitive to changes in U_B, the barotropic energy conversion increases with decreasing jet length and tends to dominate over the baroclinic conversion. For $Z \gtrsim 0.5$, the growth rate of the disturbance slowly increases monotonically with increasing Z, since longer jets (larger α) allow the disturbance to spend more time in the unstable region (for a given U_B). The existence of radiating disturbances requires that the jet length, or more precisely, the width of the locally unstable region, be sufficiently small. Although the disturbance growth rate and type of instability are sensitive to changes in jet length, particularly for short jets, the eigenmode length is much less so (not shown). Provided α (or Z) is sufficiently large, the length of the unstable region has little effect on the localization of the disturbance, but its peak amplitude shifts further downstream.

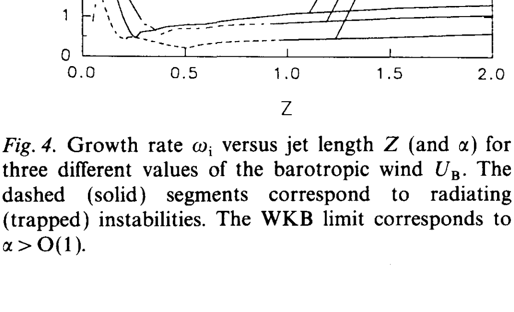

Fig. 4. Growth rate ω_i versus jet length Z (and α) for three different values of the barotropic wind U_B. The dashed (solid) segments correspond to radiating (trapped) instabilities. The WKB limit corresponds to $\alpha > O(1)$.

The structure, growth and propagation characteristics of global instabilities have been discussed in considerable detail by Pierrehumbert (1984), Cai and Mak (1990) and Whitaker and Barcilon (1992a, b) and thus are only briefly described for purposes of comparison with the local instabilities. The global instabilities are sensitive to the domain averaged baroclinicity, have growth rates that are invariant to changes in the barotropic wind, and require the zonal recycling of energy for their existence. Global instabilities are characterized by zonally propagating wave packets that undergo enhanced amplification and structural changes during the finite time that they remain within the locally unstable region. Fig. 5 shows a global eigenmode for $U_B = 1.0$ (10 m/s) and $Z = 2.0$ (2000 km) at two different times. At $t = 54$ ($62.5d$; Fig. 5a) the peak amplitude of the wave packet is located at the edge of the locally unstable region while its instantaneous growth rate is maximized at $\omega_i = 0.45$ ($0.39d^{-1}$), which is about the same as the trapped mode shown in Fig. 1. At $t = 71$ ($82.2d$; Fig. 5b) the wave packet has propagated downstream into a less unstable environment and, consequently, its instantaneous growth rate is significantly reduced to $\omega_i = -0.01$ ($-8.6 \times 10^{-3} d^{-1}$).

The combined effects of zonally uniform barotropic mean wind, $\Delta U_B = 0$, and downstream changes in vertical shear, $\Delta U_T \neq 0$, are important in determining the localization of the most unstable eigenmode. Generally, changes in eigenmode structure, growth rate and frequency arising from *increases* in downstream variations of vertical shear are qualitatively similar to those arising from *decreases* in the zonally uniform barotropic wind.

To illustrate the competition between downstream variations in vertical shear (ΔU_T) and barotropic wind (U_B) in determining the localization of the most unstable eigenmode, we show in Figs. 6a, b the boundary separating trapped, radiating and global modes for $Z = 0.2$ ($\lambda_L = 0.8$) and $Z = 2.0$ ($\lambda_L = 7.0$), respectively. As shown in Fig. 6a, large changes in downstream vertical shear and a weak barotropic wind favor trapped modes, while small changes in downstream vertical shear and a strong barotropic wind favor global modes. The radiating modes represent a transition between the trapped and global modes. The width of the transition zone decreases as both U_B and ΔU_T decrease, or as Z (or λ_L) decreases. When $U_B = 0$, values as small as $\Delta U_T = 0.3$ can support

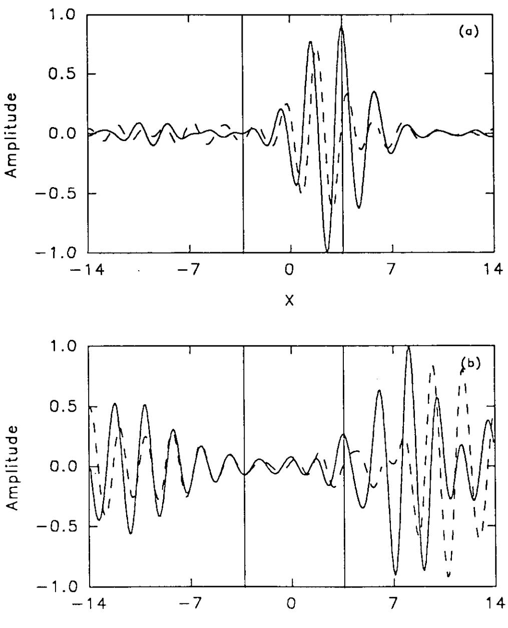

Fig. 5. The global mode corresponding to $U_B = 1.0$ and $Z = 2.0$ at two different times: (a) $t = 55$ and (b) $t = 71$.

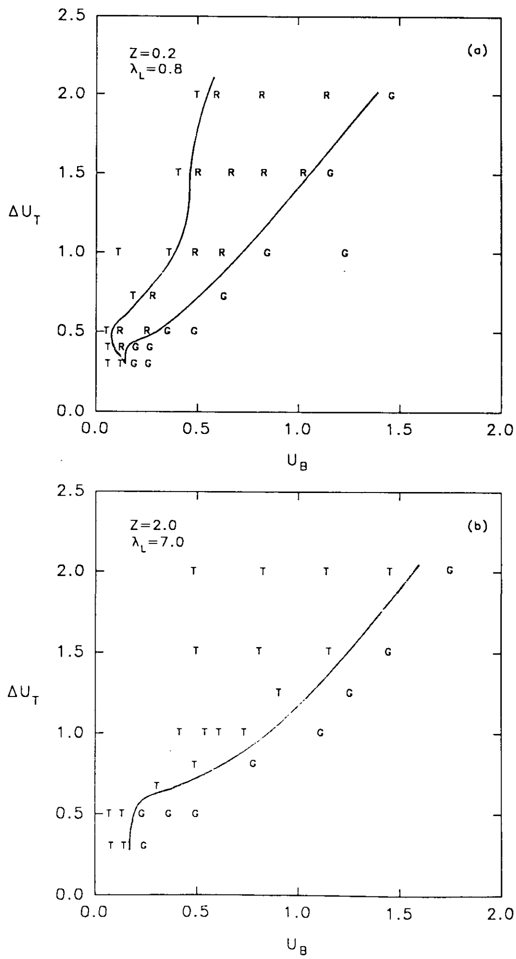

Fig. 6. The boundaries separating trapped (T), radiating (R) and global (G) modes in the ΔU_T versus U_B plane for (a) $Z = 0.2$ ($\lambda_L = 0.8$) and (b) $Z = 2.0$ ($\lambda_L = 7.0$).

local modes, where we note that for $\Delta U_T \leqslant 0.25$ all modes are neutral for this case ($U_{Tb} = 0$). This situation changes qualitatively depending on the value of the basic state vertical shear outside the jet region (U_{Tb}). In regions where the flow is locally unstable throughout the domain ($U_{Tb} > 0.25$), radiating disturbances cannot occur and the disturbances become less localized for a given value of ΔU_T than for regions where the flow is locally stable outside the jet region ($U_{Tb} < 0.25$). If the length of the locally unstable region λ_L is made sufficiently large, then radiating modes are not possible (see Fig. 6b).

The effect of changes in ΔU_T and U_B on disturbance growth rates and frequencies are shown in Fig. 7 for $Z = 0.2$ and $Z = 2.0$. The competition between ΔU_T and U_B is clearly evident; eigenmodes associated with relatively large ΔU_T (U_B) have larger (smaller) growth rates. Although increasing U_B (ΔU_T fixed) initially decreases the growth rate of the disturbance, values of $U_B \gtrsim 0.75$ yield global modes whose growth rates are insensitive to further increases in U_B (see Figs. 7a, c).

The variation of frequency with changes in ΔU_T and U_B is portrayed in Figs. 7b, d; zonal variations in vertical shear have essentially no influence on disturbance frequency, whereas increasing the barotropic wind component increases the frequency. Generally, we find that the local modes are of relatively low frequency and the global modes are of relatively high frequency, which can be attributed, in large part, to the sensitivity of the frequency to changes in U_B.

In view of the fact that the vertically averaged

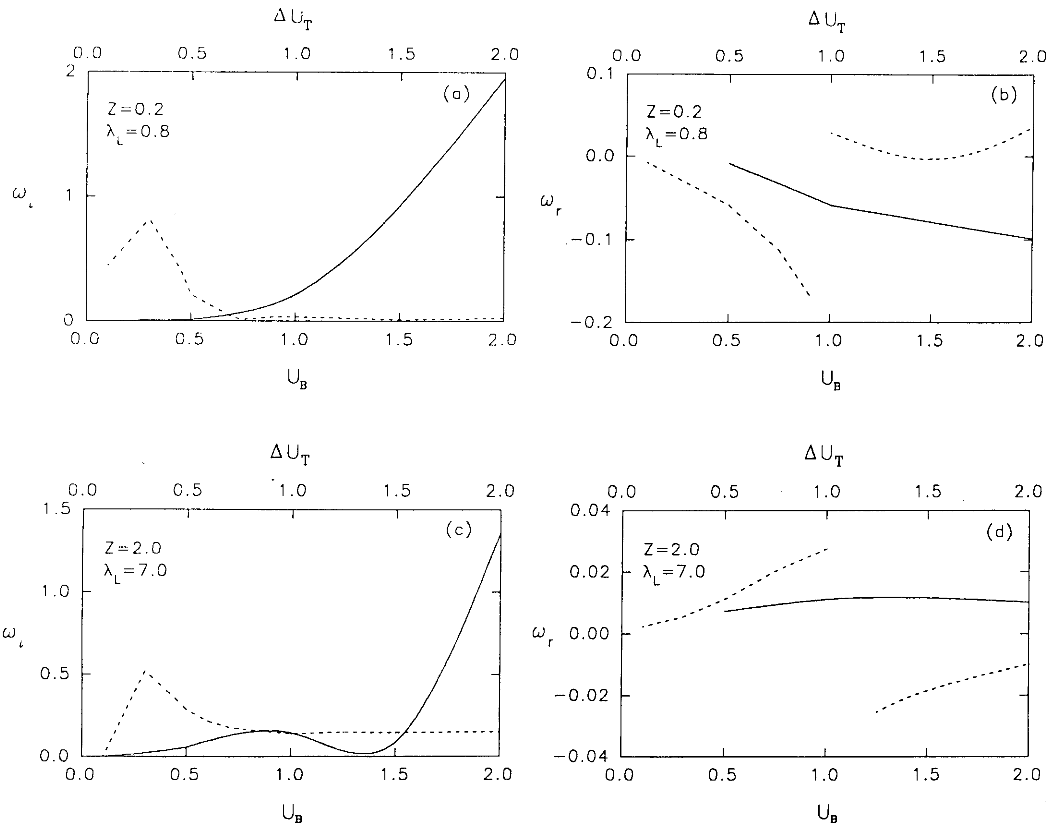

Fig. 7. The growth rate ω_i (left column) and frequency ω_r (right column) as a function of ΔU_T for $U_B = 0.5$ (solid line), and as a function of U_B for $\Delta U_T = 1.0$ (dashed line); (a), (b) $Z = 0.2$ ($\lambda_L = 0.8$) and (c), (d) $Z = 2.0$ ($\lambda_L = 7.0$). The ranges over which the modes are trapped, radiating or global can be obtained from Fig. 6.

zonal wind in the atmosphere is generally stronger in regions of enhanced baroclinicity, we have also carried out calculations in which the barotropic wind is allowed to vary zonally, such that $\Delta U_B \neq 0$ in (2.9). For Z fixed, calculations show that *increasing* the streamwise shear of the barotropic wind *reduces* the zonal scale of the disturbance, shifts its maximum amplitude closer to the jet center, and decreases its growth rate. For non-zero U_T, we find that increasing the zonal shear of the barotropic wind is dynamically equivalent to decreasing the strength of the zonally uniform barotropic wind.

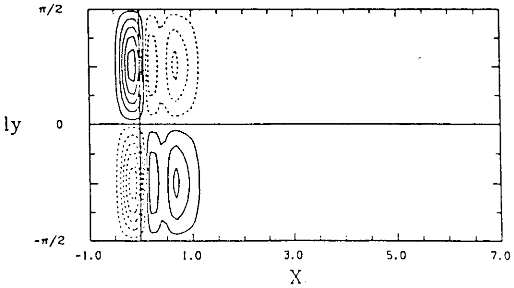

Fig. 8. Basic state barotropic vorticity tendency, $-\nabla \cdot \boldsymbol{B}$, for the trapped mode shown in Fig. 1. Maximum value normalized to 1. Contour interval 0.2.

3.4. *Basic state tendencies*

The previous section examined the linear growth and structural characteristics of baroclinic disturbances that develop within zonally varying basic states. Here we consider how these disturbances and their corresponding fluxes influence the basic state vorticity and temperature tendencies.

The initial basic state tendencies due to disturbance fluxes can be written as

$$\frac{\partial [Q_j]_e}{\partial t} = -\nabla \cdot [\boldsymbol{v}_j q_j]_e, \tag{3.7}$$

where Q_j and q_j are given by (2.2a, b), respectively, $\boldsymbol{v}_j$ is the disturbance geostrophic wind field, and the bracket $[\ ]_e$ denotes an ensemble average. Eq. (3.7) states that the time rate of change of basic state potential vorticity is due to the convergence/divergence of the disturbance potential vorticity flux.

To ease interpretation, it is convenient to separate (3.7) into barotropic and baroclinic components. Adding the upper and lower layer equations of (3.7) yields the initial basic state barotropic vorticity tendency

$$\frac{\partial [q_B]_e}{\partial t} = -\nabla \cdot \boldsymbol{B}, \tag{3.8a}$$

where $q_B = \nabla^2(\psi_1 + \psi_2)$ and

$$\boldsymbol{B} = \left[-\frac{\partial \varphi_1}{\partial y} \nabla^2 \varphi_1 - \frac{\partial \varphi_2}{\partial y} \nabla^2 \varphi_2 \right]_e \boldsymbol{i} + \left[\frac{\partial \varphi_1}{\partial x} \nabla^2 \varphi_1 + \frac{\partial \varphi_2}{\partial x} \nabla^2 \varphi_2 \right]_e \boldsymbol{j}, \tag{3.8b}$$

where $\boldsymbol{i}(\boldsymbol{j})$ are the unit vectors in the $x(y)$ directions, and $\boldsymbol{B}$ is the vertically integrated relative vorticity flux. From (3.8a), convergence of disturbance relative vorticity flux increases the ensemble averaged barotropic vorticity tendency.

Subtracting the lower-layer and upper-layer equations of (3.7) yields the baroclinic potential vorticity tendency

$$\frac{\partial [q_T]_e}{\partial t} = -\{\nabla \cdot \boldsymbol{C} - \nabla \cdot \boldsymbol{H}\}, \tag{3.9a}$$

where $q_T = (\nabla^2 - 2F)(\psi_1 - \psi_2)$,

$$\boldsymbol{C} = \left[-\frac{\partial \varphi_1}{\partial y} \nabla^2 \varphi_1 + \frac{\partial \varphi_2}{\partial y} \nabla^2 \varphi_2 \right]_e \boldsymbol{i} + \left[\frac{\partial \varphi_1}{\partial x} \nabla^2 \varphi_1 - \frac{\partial \varphi_2}{\partial x} \nabla^2 \varphi_2 \right]_e \boldsymbol{j}, \tag{3.9b}$$

$$\boldsymbol{H} = \left[F\left(-\frac{\partial \varphi_1}{\partial y} - \frac{\partial \varphi_2}{\partial y} \right) (\varphi_1 - \varphi_2) \right]_e \boldsymbol{i} + \left[F\left(\frac{\partial \varphi_1}{\partial x} + \frac{\partial \varphi_2}{\partial x} \right) (\varphi_1 - \varphi_2) \right]_e \boldsymbol{j}. \tag{3.9c}$$

The total baroclinic tendency consists of 2 parts: the thermal vorticity* tendency and the temperature tendency. For a basic state consisting of sinusoidal waves, the total baroclinic tendency is proportional to the negative of the temperature tendency. Here $\boldsymbol{C}$ is the difference between vorticity fluxes in the two layers and $\boldsymbol{H}$ contains

* The thermal vorticity is defined as the vorticity of the thermal wind.

both the zonal and meridional heat flux. The convergence of $\boldsymbol{C}$ tends to increase the ensemble averaged baroclinic vorticity tendency while the convergence of disturbance heat flux $\boldsymbol{H}$ has the opposite effect. We note that the tendency eqs. (3.8a) and (3.9a) are both $O(l)$.

Figs. 8, 9 show the basic state tendencies for the highly localized, trapped eigenmode shown in Fig. 1, where Eq. (2.5b) has been used with $l = 0.1$. Calculations also have been carried out for $l = 0.01$ yielding qualitatively similar results. Fig. 8 shows the basic state barotropic vorticity tendency, $-\nabla \cdot \boldsymbol{B}$, which is confined to a narrow region near the jet center. The net effect of the barotropic vorticity fluxes is to enhance the barotropic component of the basic state near the jet center and reduce it downstream. The downstream deceleration of the barotropic component of the flow tends to create stronger zonal basic state wind shear. Shutts (1983) obtained similar results in a barotropic model using a localized wavemaker and a strongly divergent barotropic jet. However, the acceleration of the basic state was produced by growth of the disturbance through a wavemaker, and the deceleration was due to the shearing of the disturbances by the basic state deformation field downstream of the jet core. It is interesting to note that the deceleration of the barotropic component of the flow in the baroclinic model also occurs downstream of the baroclinic jet core.

Fig. 9a shows the ensemble averaged temperature tendency produced by the trapped mode. For the most part, the effects of the disturbance are confined to within ~ 1000 km of the jet center. The temperature tendency shows warming (cooling) to the north (south) of the jet center, about 500 km upstream and about 700 km downstream of the jet center indicating that the disturbance is acting to destroy the basic state north-south temperature gradient in these areas. About 200 km upstream of the jet center, the temperature tendency shows cooling to the north of the jet and warming to the south indicating that the disturbance fluxes are enhancing the meridional temperature gradient in the jet entrance region.

The total baroclinic tendency of the trapped mode is shown in Fig. 9b. Areas where the baroclinic tendency increases (decreases) with y are areas where the vertical wind shear tendency is positive (negative). Fig. 9b shows that the fluxes created by the highly localized trapped mode tend to increase the basic state vertical wind shear in the jet entrance region, and decrease the vertical wind shear in the jet exit region and in regions ~ 700 km west and ~ 1000 km east of the jet center.

As discussed in Subsection 3.3, radiating modes extend well beyond the locally unstable region. The barotropic vorticity tendency corresponding to the radiating mode shown in Fig. 2 is shown

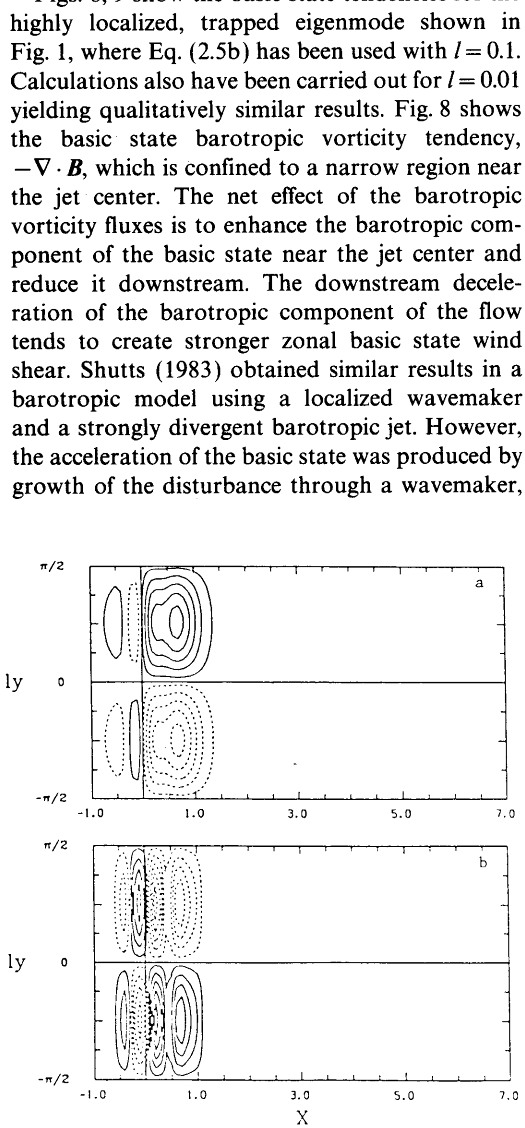

Fig. 9. (a) Temperature tendency, $\partial[\psi_1 - \psi_2]_e/\partial t$, and (b) total basic state baroclinic tendency, $\partial[q_T]_e/\partial t$, for the trapped mode shown in Fig. 1. Maximum value normalized to 1. Contour interval 0.2. Solid/dashed lines correspond to positive/negative values.

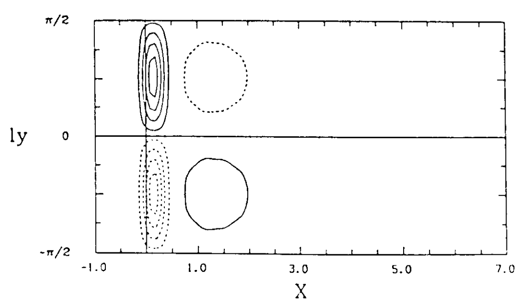

Fig. 10. Basic state barotropic vorticity tendency, $-\nabla \cdot \boldsymbol{B}$, for the radiating mode shown in Fig. 2. Maximum value normalized to 1. Contour interval 0.2. Solid/dashed lines correspond to positive/negative values.

in Fig. 10. As expected, the barotropic vorticity fluxes for the radiating disturbance extend further downstream than those of the trapped mode. Maximum basic state barotropic tendencies lie in the jet exit region, indicating an acceleration in the basic state barotropic wind, while ~ 1200 km downstream of the jet center, the barotropic tendency indicates a deceleration in the basic state barotropic wind, although this deceleration is considerably smaller than that found for the trapped disturbance.

Fig. 11 shows the basic state temperature and total baroclinic tendency produced by the radiating mode. The heat flux (not shown) is predominantly northward and maximized ~ 1500 km downstream of the jet center. The temperature tendency (Fig. 11a), which is positive (negative) to the north (south) of the jet, extends well beyond the locally unstable region; the disturbance heat fluxes reduce the meridional temperature gradient in the jet region and as far as ~ 2700 km downstream of the jet center, in contrast to the trapped mode whose heat fluxes were confined within ~ 1000 km of the jet center. The total baroclinic tendency (Fig. 11b) is predominantly negative (positive) to the north (south) of the jet, and, like the temperature tendency, displays a slight zonal elongation typical of the radiating modes. Compare this with the baroclinic tendencies for trapped mode (Fig. 9b). While the fluxes produced by the trapped mode tend to reinforce the jet, the radiating mode produces fluxes that tend to weaken the vertical shear both in the jet region and downstream from the jet.

The basic state tendencies for $Z = 2.0$ ($\lambda_L = 7.0$, $\alpha = 3.5$), which correspond to the WKB limit, are shown in Figs. 12, 13. The results are qualitatively similar to those obtained by Pierrehumbert (1986) and thus will only be briefly summarized. Fig. 12 shows the barotropic vorticity tendency associated with the eigenmode shown in Figs. 3b, d and f. There is weak barotropic vorticity flux convergence (divergence) to the noth (south) of the jet exit region, inducing a slight deceleration in the barotropic component of the flow downstream of the jet core, which tends to zonally extend the jet and create zonal shear in the basic state.

The temperature tendency and total baroclinic vorticity tendency are shown in Fig. 13. The temperature tendency is maximized ~ 2000 km downstream of the jet center, with warming occurring to the north of the jet, cooling to the south. Thus the disturbance heat flux tends to reduce the pre-existing north-south temperature gradient *downstream* of the peak meridional temperature gradient. The position of maximum northward heat flux depends strongly on the structure of the eigenmode and its position relative to the jet, which is sensitive to U_B. Those distur-

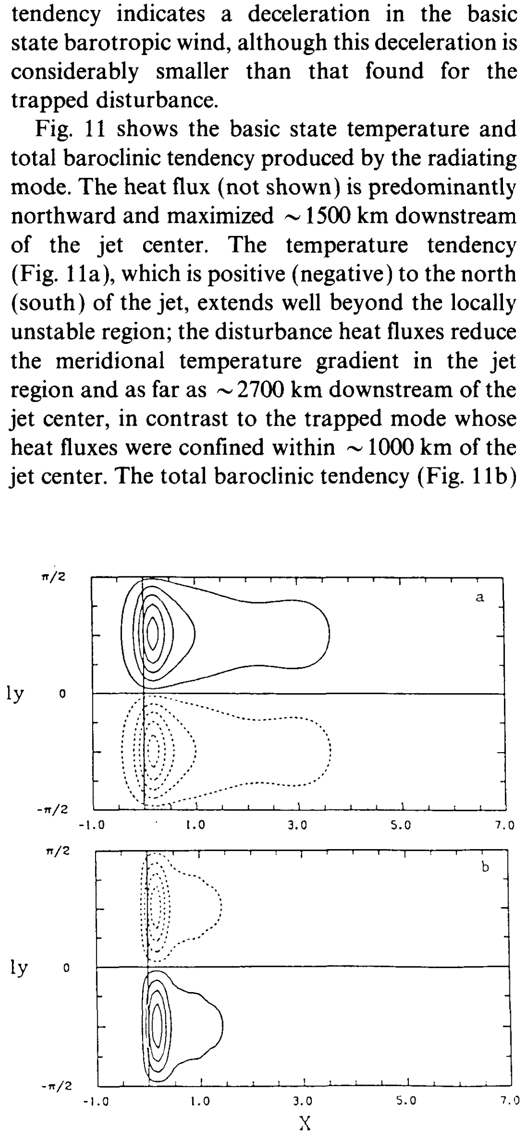

Fig. 11. (a) Temperature tendency, $\partial[\psi_1 - \psi_2]_e/\partial t$, and (b) total basic state baroclinic tendency, $\partial[q_T]_e/\partial t$, for the radiating mode shown in Fig. 2. Maximum value normalized to 1. Contour interval 0.2. Solid/dashed lines correspond to positive/negative values.

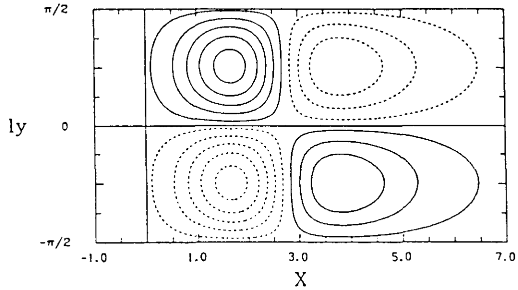

Fig. 12. Basic state barotropic vorticity tendency, $-\nabla \cdot \boldsymbol{B}$, for the trapped mode shown in Fig. 3b. Maximum value normalized to 1. Contour interval 0.2. Solid/dashed lines correspond to positive/negative values.

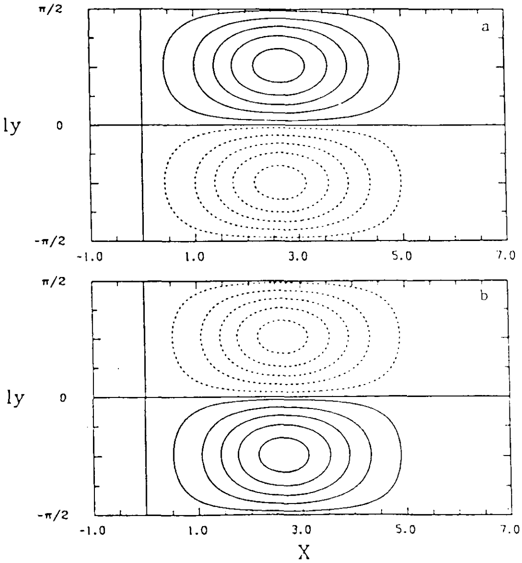

Fig. 13. (a) Temperature tendency, $\partial[\psi_1 - \psi_2]_e/\partial t$, and (b) total basic state baroclinic tendency, $\partial[q_T]_e/\partial t$, for the trapped mode shown in Fig. 3b. Maximum value normalized to 1. Contour interval 0.2. Solid/dashed lines correspond to positive/negative values.

bances with peak amplitudes near the jet center produce strong northward heat fluxes there which tend to weaken the vertical shear, whereas those disturbances with maximum amplitudes far downstream from the jet center produce heat fluxes which tend to reinforce the zonal inhomogeneities in the basic state vertical shear. The basic state tendencies indicate that the net effect of the disturbances is to redistribute energy from the baroclinic to the barotropic component of the basic state flow. This redistribution is only possible in the two-layer model if the basic state zonal winds in the upper (lower) layer decrease (increase) from their initial values. This result is consistent with the findings of Lau and Holopainen (1984) who showed that disturbance poleward heat transports produced eastward (westward) accelerations in the geostrophic winds in the lower (upper) troposphere.

Finally, we note that a zonally varying barotropic wind enhances localization of the disturbance fluxes and concentrates them closer to the jet core where they act to enhance downstream changes in the barotropic wind and destroy zonal inhomogeneities in the basic state vertical wind shear.

4. Concluding remarks

The baroclinic instability characteristics of zonally inhomogeneous flow have been examined using the conventional quasigeostrophic, two-layer, beta-plane model. Under the assumption that the disturbance varies slowly in the cross-stream direction, the stability problem was cast in the form of a one dimensional initial value problem in which the most unstable eigenmode was determined numerically. Emphasis has been placed on determining how the vertically averaged wind U_B, local maximum in vertical wind shear ΔU_T, and length of the locally supercritical region λ_L, combine to yield local instabilities whose energy fluxes penetrate deep into the locally neutral far field. The emergence of such radiating instabilities (RI), which represent a transition between trapped and global instabilities, requires that λ_L not exceed some critical value and that $\Delta U_T/U_B$ lie within a certain range. In sharp contrast to the trapped and global instabilities, the RI have zonal wavelengths that increase dramatically with distance from the locally unstable region owing to the excitation of the Rossby wave in the far field. If the width of the locally supercritical region is sufficiently narrow and the barotropic wind sufficiently weak, the local instability that emerges is characterized by a vertical asymmetry in its *horizontal* spatial structure; the upper layer disturbance has a longer zonal scale than its counterpart in the lower layer.

An analysis of the local energetics has revealed that for slowly varying zonal flows, a parameter setting that yields only trapped or global instabilities, the baroclinic energy conversion predominates within the locally unstable region, whereas for relatively rapid variations in the zonal flow, the barotropic energy conversion associated with the horizontal deformation field may predominate depending on the value of U_B, which plays a vital role in determining the structure, growth rate and frequency of the eigenmode. For radiating instabilities, the energy budget outside the locally unstable region is due to the advection of total energy and the convergence of mechanical energy flux, which slowly decay with distance from the source.

The basic state tendencies have also been calculated and show that the ensemble averaged wave fluxes of the local (trapped and radiating) instabilities act to redistribute energy from the baroclinic to the barotropic part of the flow. The baroclinic wave fluxes of the trapped instabilities are typically maximized downstream of the jet center and therefore maintain the zonal nonuniformity in the meridional temperature gradient and thus vertical wind shear. In contrast, the radiating instabilities produce wave fluxes that tend to reduce the baroclinicity (vertical wind shear) both within and downstream of the jet center.

The trapped modes are generally favored when changes in the downstream vertical shear are large and the barotropic wind is weak, i.e., the trapped modes arise when $\Delta U_T > U_B$, which corresponds to easterlies in the lower layer. However, the *climatological* distribution of the zonal wind at middle latitudes is westerly throughout the troposphere. Thus, to the extent that the model atmosphere used here is representative of the real atmosphere, the global modes should be favored for typical midlatitude flows. These results are consistent with those obtained by Whitaker and Barcilon (1992b), who demonstrated that for zonally modulated, vertically sheared zonal flows, only baroclinically unstable global modes emerge. Therefore, local (trapped or radiating) modes are more apt to be observed during large-scale blocking episodes, i.e., when the surface winds have a greater likelihood of being easterly. However, the generality of this conclusion must await further confirmation in more realistic models, since the model used here, and that of Whitaker and Barcilon, have neglected meridional variations in the basic state and disturbance fields. It is entirely possible that the inclusion of such variations may permit local instabilities to develop on vertically sheared, westerly flows.

Finally, we note that although our study has focused on the stability properties of zonally varying flows in the atmosphere, our results are equally relevant to the ocean and other geophysical fluid systems that possess zonal variations in baroclinicity. We must emphasize, however, that the model used in this study is highly idealized. We have not considered zonally (or meridionally) asymmetric jets which, as stated above, could significantly change the stability properties of the basic state flow. Moreover, our analysis of the initial value problem has allowed us to focus only on the most unstable eigenmode; the additional unstable modes that might be obtained via an eigenvalue problem approach also are of physical interest. Finally, nonlinear effects must be considered in order to provide a comprehensive description of the life cycles of disturbances arising from the instability of zonally inhomogeneous flow. In particular, it would be interesting to see if the continuous radiation and advection of energy from the locally unstable region could lead to substantial secondary development at the expense of the primary development that occurs within the locally unstable baroclinic zone. Such problems are currently under investigation.

5. Acknowledgments

The authors thank two anonymous reviewers for their helpful comments on the manuscript. Thanks also are due Mr. Long Li and Mr. Ken Sperow for their many helpful discussions on this work and for providing valuable assistance in the preparation of the figures. This work was supported by National Science Foundation Grant ATM-90-96153 and by National Aeronautics and Space Administration Grants NAG8-811 and NAG8-871. Acknowledgment also is made to the National Center for Atmospheric Research, which is sponsored by the National Science Foundation, for the computer time used in this research.

6. Appendix

Derivation of the local energetics eq. (2.7)

Multiplying the inviscid form of (2.1) by $-\varphi_j$ and summing over the two layers yields,

$$\frac{\partial}{\partial t}\left(\sum_{j=1}^{2} K_j + P\right) = \sum_{j=1}^{2}\left\{\frac{\partial}{\partial x}\left[\varphi_j \frac{\partial v_j}{\partial t}\right] - \frac{\partial}{\partial y}\left[\varphi_j \frac{\partial u_j}{\partial t}\right] + \varphi_j[\boldsymbol{V}_j \cdot \nabla q_j + \boldsymbol{v}_j \cdot \nabla Q_j]\right\}, \quad \text{(A1)}$$

where Q_j and q_j are defined by eqs. (2.2a, b); the basic state and disturbance wind fields are, respectively,

$$\boldsymbol{V}_j(x, y) = U_j(x, y)\boldsymbol{i} + V_j(x, y)\boldsymbol{j} = -\frac{\partial \bar{\psi}_j}{\partial y}\boldsymbol{i} + \frac{\partial \bar{\psi}_j}{\partial x}\boldsymbol{j} \quad \text{(A2)}$$

$$\boldsymbol{v}_j = u_j(x, y)\boldsymbol{i} + v_j(x, y)\boldsymbol{j}$$
$$= -\frac{\partial \varphi_j}{\partial y}\boldsymbol{i} + \frac{\partial \varphi_j}{\partial x}\boldsymbol{j}, \tag{A3}$$

where $\boldsymbol{i}(\boldsymbol{j})$ are the unit vectors in the $x(y)$ directions. The disturbance kinetic and potential energies are given by $K_j = (u_j^2 + v_j^2)/2$ and $P = F(\varphi_1 - \varphi_2)^2/2$, respectively. If we define

$$(\varphi_\mathrm{T}, \varphi_\mathrm{B}) = [(\varphi_1 - \varphi_2), (\varphi_1 + \varphi_2)], \tag{A4}$$

$$(U_\mathrm{T}, U_\mathrm{B}) = (U_1 - U_2, U_1 + U_2), \tag{A5}$$

$$(V_\mathrm{T}, V_\mathrm{B}) = (V_1 - V_2, V_1 + V_2), \tag{A6}$$

and use the fact that the geostrophic wind is non-divergent, i.e., $\nabla \cdot \boldsymbol{V}_j = 0$, eq. (A1) can be written as,

$$\frac{\partial}{\partial t}\left(\sum_{j=1}^{2} K_j + P\right) = \sum_{j=1}^{2}\left\{ -\boldsymbol{V}_j \cdot \nabla K_j - 2\boldsymbol{V}_\mathrm{B} \cdot \nabla P \right.$$
$$- 2F\varphi_\mathrm{B}\nabla \cdot (\boldsymbol{V}_\mathrm{T}\varphi_\mathrm{T}) + \varphi_j \boldsymbol{v}_j \cdot \nabla Q_j$$
$$+ \frac{\partial}{\partial x}\left[\varphi_j\left(\frac{\partial v_j}{\partial t} + U_j\frac{\partial v_j}{\partial x}\right)\right] - \varphi_j\frac{\partial}{\partial x}\left(U_j\frac{\partial u_j}{\partial y}\right)$$
$$\left. - \frac{\partial}{\partial y}\left[\varphi_j\left(\frac{\partial u_j}{\partial t} + V_j\frac{\partial u_j}{\partial x}\right)\right] - \varphi_j\frac{\partial}{\partial x}\left(V_j\frac{\partial v_j}{\partial y}\right)\right\}. \tag{A7}$$

To eliminate the time derivatives on the right-hand side, we use the zonal and meridional momentum equations:

$$\frac{\partial u_j}{\partial t} + V_j\frac{\partial u_j}{\partial y} = -U_j\frac{\partial u_j}{\partial x} - u_j\frac{\partial U_j}{\partial x} - v_j\frac{\partial U_j}{\partial y}$$
$$- \frac{\partial \phi_j'}{\partial x} + v_j' - v_j\beta y, \tag{A8}$$

$$\frac{\partial v_j}{\partial t} + U_j\frac{\partial v_j}{\partial x} = -V_j\frac{\partial v_j}{\partial y} - u_j\frac{\partial V_j}{\partial x} - v_j\frac{\partial V_j}{\partial y}$$
$$- \frac{\partial \phi_j'}{\partial y} - u_j' - u_j\beta y, \tag{A9}$$

where ϕ_j' and (u_j', v_j') represent the ageostrophic pressure and wind fields, respectively. Insertion of (A8) and (A9) into (A7) yields,

$$\frac{\partial}{\partial t}\left(\sum_{j=1}^{2} K_j + P\right) = -\sum_{j=1}^{2}[\boldsymbol{V}_j \cdot \nabla K_j + \boldsymbol{V}_\mathrm{B} \cdot \nabla P]$$
$$- \sum_{j=1}^{2}\nabla \cdot (\boldsymbol{v}_j\phi' + \varphi\boldsymbol{v}_j') + \sum_{j=1}^{2}\boldsymbol{E}_j \cdot \boldsymbol{D}_j$$
$$+ 2F[U_\mathrm{T}\varphi_\mathrm{T}v_\mathrm{B} - V_\mathrm{T}\varphi_\mathrm{T}u_\mathrm{B}], \tag{A10}$$

where

$$\boldsymbol{E}_j = \tfrac{1}{2}(v_j^2 - u_j^2)\,\boldsymbol{i} + u_j v_j \boldsymbol{j}, \tag{A11}$$

$$\boldsymbol{D}_j = \left(\frac{\partial U_j}{\partial x} - \frac{\partial V_j}{\partial y}\right)\boldsymbol{i} + \left(\frac{\partial V_j}{\partial x} + \frac{\partial U_j}{\partial y}\right)\boldsymbol{j}. \tag{A12}$$

Eq. (A10) represents the vertically averaged, local disturbance energy equation valid for an arbitrary basic flow. Eq. (2.7) is obtained by substituting (2.5) into (A10), setting $l \ll 1$ and averaging in y.

Calculation of the second term on the right-hand side of (10), which represents the convergence of mechanical energy flux, requires knowledge of the ageostrophic pressure and wind fields. This information can be obtained by combining the mass continuity equation (not shown) and momentum eqs. (A8 and A9) to obtain a *diagnostic* partial differential equation for the ageostrophic pressure field. However, multiplying (A8) by u_j and (A9) by v_j and adding the two equations, the convergence of mechanical energy flux can be calculated solely in terms of the geostrophic pressure field. This was the approach taken to calculate term C in (2.7).

REFERENCES

Andrews, D. G. 1984. On the stability of forced nonzonal flows. *Q. J. R. Meteorol. Soc. 110*, 657–662.

Cai, M. and Mak, M. 1990. On the basic dynamics of regional cyclogenesis. *J. Atmos. Sci. 47*, 1417–1442.

Crum, F. X. and Stevens, D. E. 1990. Barotropic instability with downstream variations and asymmetric cross-stream variations: Idealized calculations. *J. Atmos. Sci. 47*, 5–23.

Frederiksen, J. S. 1979. The effect of long planetary waves on the regions of cyclogenesis: Linear theory. *J. Atmos. Sci. 36*, 195–204.

Frederiksen, J. S. 1983. Disturbances and eddy fluxes in

Northern Hemisphere flows: instability of three-dimensional January and July flows. *J. Atmos. Sci. 40*, 836–855.

Grotjahn, R. 1984. Baroclinic instability in a long wave environment. Part II: Ageostrophic energy conversions. *Quart. J. R. Met. Soc. 110*, 669–693.

Howell, P. and Nathan, T. R. 1990. Barotropic instability of zonally varying flow forced by multimode topography. *Dyn. Atmos. Oceans 15*, 35–58.

Lau, N.-C. and Holopainen, E. 1984. Transient eddy forcing of the time-mean flow as identified by geopotential tendencies. *J. Atmos. Sci. 41*, 313–328.

Manney, G. L. and Nathan, T. R. 1990. Barotropic stability of westward, moving waves in realistic stratospheric zonal flows. *J. Atmos. Sci. 47*, 775–794.

McIntyre, M. E. and Weissman, M. A. 1978. On radiating instabilities and resonant overreflection. *J. Atmos. Sci. 35*, 1190–1196.

Neihaus, M. C. W. 1981. Instability of non-zonal baroclinic flows: Multiple scale analysis. *J. Atmos. Sci. 38*, 974–987.

Orlanski, I. and Katzfey, J. 1991. The life cycle of a cyclone wave in the Southern Hemisphere. Part I: Eddy Energy Budget. *J. Atmos. Sci. 48*, 1972–1998.

Pedlosky, J. 1987. *Geophysical fluid dynamics.* Second Edition. Springer-Verlag, 710 pp.

Peng, M. and Williams, R. T. 1984. Spatial instability of a baroclinic current with slow streamwise variation. *J. Atmos. Sci. 44*, 1681–1695.

Phillips, N. A. 1954. Energy transformations and meridional circulations associated with simple baroclinic waves in a two-level, quasi-geostrophic model. *Tellus 6*, 273–286.

Pierrehumbert, R. T. 1984. Local and global baroclinic instability of zonally varying flow. *J. Atmos. Sci. 41*, 2141–2162.

Pierrehumbert, R. T. 1986. The effects of local baroclinic instability on zonal inhomogeneities of vorticity and temperature. *Adv. Geophys. 29*, 165–182.

Samelson, R. and Pedlosky, J. 1990. Local baroclinic instability of flow over variable topography. *J. Fluid Mech. 221*, 411–436.

Shutts, G. J. 1983. The propagation of eddies in diffluent jetstreams: eddy vorticity forcing of blocking flows. *Quart. J. Roy. Meteor. Soc. 109*, 737–761.

Talley, L. D. 1983. Radiating instabilities of thin baroclinic jets. *J. Phys. Ocean 13*, 2161–2181.

Whitaker, J. S. and Barcilon, A. 1992a. Genesis of mobile troughs in the upper westerlies. *J. Atmos. Sci. 49*, 2097–2107.

Whitaker, J. S. and Barcilon, A. 1992b. Type B cyclogenesis in a zonally varying flow. *J. Atmos. Sci. 49*, 1877–1892.